

Bandwidth Extension of Dual-Polarized 1-D TCDA Antenna Using VMS

Seongjung Kim¹, and Sangwook Nam¹, *Senior Member, IEEE*

Abstract—In this paper, a wideband, low-profile, 1-D tightly coupled dipole array (1-D TCDA) antenna with vertical metal strips (VMSs) is proposed. The 1-D TCDA has a limited scanangle due to variations in vertical wave numbers according to the scanangle. Floquet theory and the electric field profile can be used to analyze the theory of a TCDA, obtaining scan-independent characteristic. Removing some metal strips from the side walls also improved the radiation efficiency. The overlapped impedance bandwidth (IBW) for dual polarization was 0.8–2.5 GHz (3.1:1) for VSWR < 3, and the maximum scanangle was $\pm 50^\circ$. The radiation efficiency was over 70% within the IBW and maximum scanangle. The measurement results show that the gain was 7.0–12.4 dB for vertical polarization and 7.3–15.4 dB for horizontal polarization within the IBW and maximum scanangle. Furthermore, the height of the antenna was $0.13\lambda_{\text{low}}$ at the lowest operating frequency, and the overall dimension of the full array structure was $1.69\lambda_{\text{low}} \times 0.59\lambda_{\text{low}} \times 0.13\lambda_{\text{low}}$.

Index Terms—Low-profile antenna, phased array antenna, radiation efficiency, tightly coupled dipole array (TCDA), wideband antenna, wide scannable antenna.

I. INTRODUCTION

WIDEBAND phased array antennas are widely used in many applications, such as communication systems, radar systems, and electronic warfare antennas. Phased array antennas can steer the main beam and provide communication links in different directions. A tapered slot array (TSA) antenna or Vivaldi array antenna is a well-known extremely wideband array antenna [1]–[5]. However, the height of this antenna is lofty because it supports traveling waves. On the other hand, the microstrip type can be an extremely low-profile array antenna but the bandwidth is very narrow [6].

The 2-D tightly coupled dipole array (TCDA) antenna has been proposed to implement low-profile array antennas [7]. The TCDA is a dense array of dipoles that overlap each other to imitate a current sheet array (CSA) for wide bandwidth [8]. It has wideband and good scan performance [9]–[11]. However, its applications are limited because it can only be implemented as a 2-D array. Thus, in recent years, 1-D TCDA versions have been proposed [12]–[15]. The 1-D array

antenna can be used for many applications, such as base station antennas. By establishing impedance surface walls on both sides, Lee and Nam [12] found that the dual-polarized 2-D TCDA can be reduced to a 1-D TCDA. Folded dipoles and vertical ground planes were used in [13] to compensate for the coupling capacitance, and a single-polarized TCDA was proposed in [14], using parasitic metal strips on dipole antennas for wide impedance bandwidth (IBW). Extremely broadband 1-D TCDA (30:1) has been proposed for body-worn applications [15], which is possible as it does not have any horizontal metallic ground plane.

However, the boundary condition of the extant 1-D TCDA [12] is imperfect, especially when scanning the beam. When scanning the beam, the impedance matching becomes poor. In 2-D cases, many efforts [16]–[18] have been made to have a wide scan-angle performance, with light weight and low cost. Wide angle impedance matching (WAIM) was proposed in [16]. A high dielectric constant slab is placed over the antennas. However, when the slab is placed at a proper position, the height inevitably becomes lofty and the bandwidth becomes narrower. An advanced version of WAIM, with a metasurface, was used in [17] to steer the beam more widely. However, it still has a lofty height and the bandwidth is narrow. By placing a frequency selective surface (FSS) on dipole antennas, Yetisir *et al.* [18] found that the beam can be steered up to $\pm 70^\circ$. Therefore, in the 1-D case, the antenna [13] used this FSS for both polarizations, and it can steer the beam up to $\pm 60^\circ$. However, the greatest disadvantage of FSS is that its height is lofty.

In this paper, the proposed antenna has been designed based on the one described in [12]. Compared with the 1-D TCDA in [12], it is clear that this work is better in terms of beam scanning and impedance matching property. Also, Wilkinson power divider/combiner is used for the feeding structure in [13] and [14], which makes the antenna height larger even though the bandwidth can be wider. The main purpose of this paper is to propose a method for wide beam scanning or for a low-profile array antenna. The degradation of impedance matching with beam scanning is discussed, and the effect of vertical metal strip (VMS) on phased array is presented. The main reason for the impedance mismatch, especially at the low-frequency band, is analyzed carefully by the Floquet theory and the electric field profile. By placing the VMS under the dipole, the impedance matching is improved at a low-frequency band. The concept of VMS is expected to be applicable not only for TCDA but also for many other phased array antennas.

Manuscript received December 12, 2018; revised April 6, 2019; accepted May 3, 2019. Date of publication May 20, 2019; date of current version August 12, 2019. This work was supported by the Global Frontier Program through the National Research Foundation of Korea (NRF) funded by the Ministry of Science, ICT & Future Planning under Grant NRF-2014M3A6B3063708. (*Corresponding author: Seongjung Kim.*)

The authors are with the Institute of New Media Communication (INMC), School of Electrical and Computer Engineering, Seoul National University, Seoul 08826, South Korea (e-mail: sjkim@ael.snu.ac.kr; snam@snu.ac.kr).

Color versions of one or more of the figures in this paper are available online at <http://ieeexplore.ieee.org>.

Digital Object Identifier 10.1109/TAP.2019.2916745

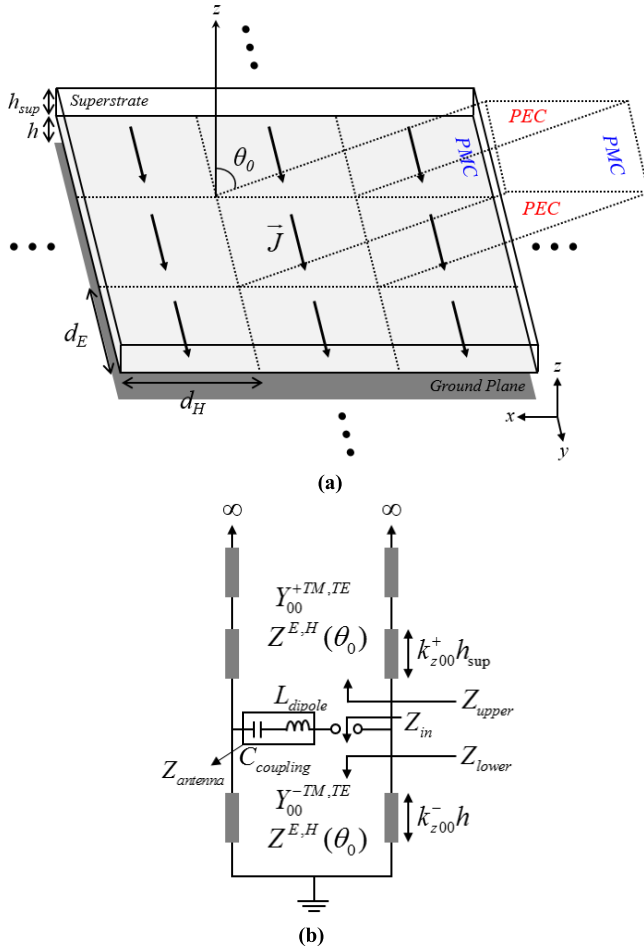


Fig. 1. (a) Ideal boundary condition of the unit cell of a TCDA when scanning to $\theta = \theta_0$. (b) Equivalent circuit of the unit cell.

The rest of this paper is organized as follows. Section II introduces the theory of a 2-D and 1-D TCDA. Section III shows the configuration of the proposed array antenna, including its operating principle. Section IV presents the experimental results for the proposed array antenna and the table of performance comparisons. Section V offers conclusions drawn from the findings.

II. THEORY OF A 2-D AND 1-D TCDA

A. Theory of a 2-D TCDA

This section introduces the theory of a 2-D TCDA. Fig. 1(a) shows the boundary condition of a unit cell of a TCDA simulating a uniform current sheet [19]; Fig. 1(b) shows the equivalent circuit of the unit cell. The unit cell can be seen in a PEC/PMC waveguide, and the waveguide is steered when feeding the elements by different phases. L_{dipole} represents a self-inductance of the dipole, and $C_{coupling}$ represents a gap capacitance between the dipoles. $Z^{E,H}(\theta_0)$ and k_{z00} are the characteristic impedance and fundamental propagation mode to the z -direction, respectively, which can be changed by conditions such as scanangles, materials, and operating frequencies. To express them, the information about a material and a beam scanangle is required. The modal admittances of

the fundamental TE and TM Floquet modes, given in [20], are the following, respectively:

$$Y_{00}^{TE+} = \frac{k_{z00}^+}{\omega\mu_0}, \quad Y_{00}^{TE-} = \frac{k_{z00}^-}{\omega\mu_0} \quad (1)$$

$$Y_{00}^{TM+} = \frac{\omega\epsilon_0\epsilon_r}{k_{z00}^+}, \quad Y_{00}^{TM-} = \frac{\omega\epsilon_0}{k_{z00}^-}. \quad (2)$$

The superscripted positive sign represents the positive z direction, and the superscripted negative sign represents the negative z direction. Furthermore, ϵ_r is the relative dielectric constant, which is to be ϵ_{sup} in the superstrate and 1 in free space. For both modes, $k_{z00}^+ = \sqrt{\epsilon_r k_0^2 - k_{x00}^2 - k_{y00}^2}$ and $k_{z00}^- = \sqrt{k_0^2 - k_{x00}^2 - k_{y00}^2}$, where k_0 is the wave number in free space.

In this configuration, when the beam is steered in the H- and E-planes, the TE mode and TM mode, respectively, are dominant. In fact, the TE and TM modes exist simultaneously when scanning the beam to a direction outside the H- and E-planes. When scanning the beam in the H- and E-planes, the characteristic impedances of the transmission lines, expressed in [21], are the following, respectively:

$$Z^H(\theta_0) = \frac{d_E}{d_H} \frac{1}{Y_{00}^{TE}} = \eta_0 \sqrt{\frac{\mu_r}{\epsilon_r}} \frac{d_E}{d_H} \frac{1}{\cos\theta_0} \quad (3)$$

$$Z^E(\theta_0) = \frac{d_E}{d_H} \frac{1}{Y_{00}^{TM}} = \eta_0 \sqrt{\frac{\mu_r}{\epsilon_r}} \frac{d_E}{d_H} \cos\theta_0 \quad (4)$$

where θ_0 is the beam's scanangle, η_0 is the characteristic impedance in free space, and μ_r is the relative permeability. Moreover, d_E and d_H are the length of the unit cell denoted in Fig. 1(a)

$$Z_{in} = Z_{antenna} + Z_{upper} \parallel Z_{lower} \quad (5)$$

$$Z_{antenna} = j\omega L_{dipole} + \frac{1}{j\omega C_{coupling}} \quad (6)$$

$$Z_{upper} = Z^{E,H}(\theta_0) \frac{\sqrt{\epsilon_{sup}} + j \tan(k_{z00}^+ h_{sup})}{1 + j \sqrt{\epsilon_{sup}} \tan(k_{z00}^+ h_{sup})} \Big|_{\epsilon_r = \epsilon_{sup}, \mu_r = 1} \quad (7)$$

$$Z_{lower} = j Z^{E,H}(\theta_0) \tan(k_{z00}^- h) \Big|_{\epsilon_r = 1, \mu_r = 1} \quad (8)$$

where ω is the operating angular frequency and h is the spacing between the dipole and the ground plane.

The operating principle of the TCDA is based on the impedance matching at a low-frequency band, which indicates the implementation of a low-profile antenna. At a low-frequency band, Z_{lower} is inductive because of the ground plane. However, this is compensated by the gap coupling $C_{coupling}$. At a high frequency, Z_{lower} is capacitive and compensated by self-inductance L_{dipole} . As a result, from a low-frequency band to a high-frequency band, Z_{in} can be matched.

Note that in (8), $k_{z00}^- h = k_0 h \cos\theta_0$ is a function not only of the beam's scanangle but also of the beam's frequency. Therefore, Z_{lower} is a function of the frequency and the beam scanangle. When the beam is steered along the E- or H-plane, the Z_{lower} goes to zero, which is a similar effect to operating at a lower frequency band. Nevertheless, beam scanning along

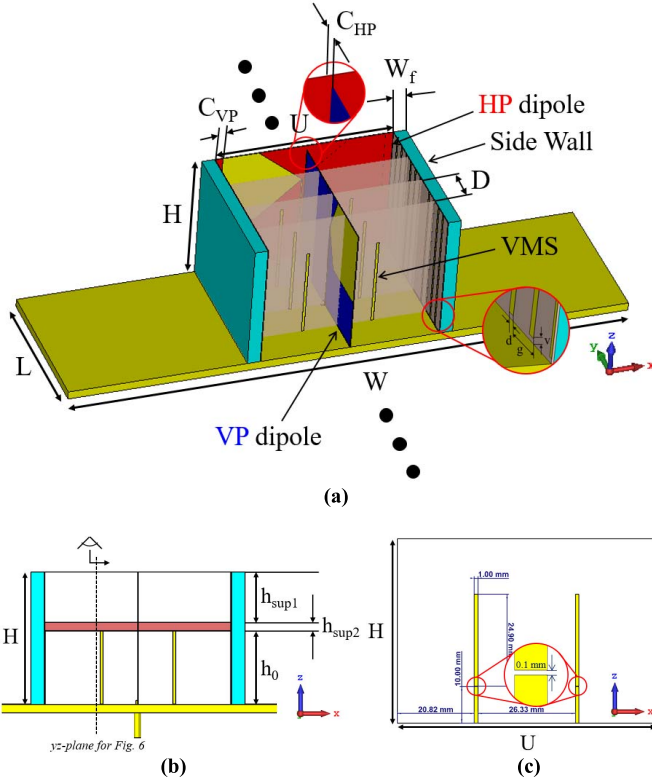


Fig. 2. (a) Dimensions of the proposed unit cell antenna without superstrates. (b) Description of the front side. (c) Description of the VMSs. (d) Configuration of the full array structure (10 VP elements and 11 HP elements, overall dimensions: $635 \times 220 \times 50 \text{ mm}^3$).

the H-plane is less sensitive than it is along the E-plane due to the $1/\cos \theta_0$ term in (3). As a result, because Z_{upper} also varies with the frequency and beam scanangle, but $Z_{upper} // Z_{lower}$ is dominated by Z_{lower} when the beam is steered in the E-plane at a low-frequency band, the impedance matching (5) becomes very poor.

Section III-B presents our solution to this problem.

B. Theory of a 1-D TCDA

To reduce the dimensions of a dual-polarized 2-D TCDA to a dual-polarized 1-D TCDA, an impedance surface wall must be established on both sides, as shown in Fig. 2(d), and satisfy the boundary condition for both polarizations [12]. The impedance wall comprises metal strips and a ferrite sheet, as shown in Fig. 4(a). Metal strips only satisfy the boundary condition of HP dipoles (x -direction polarized) as a PEC wall,

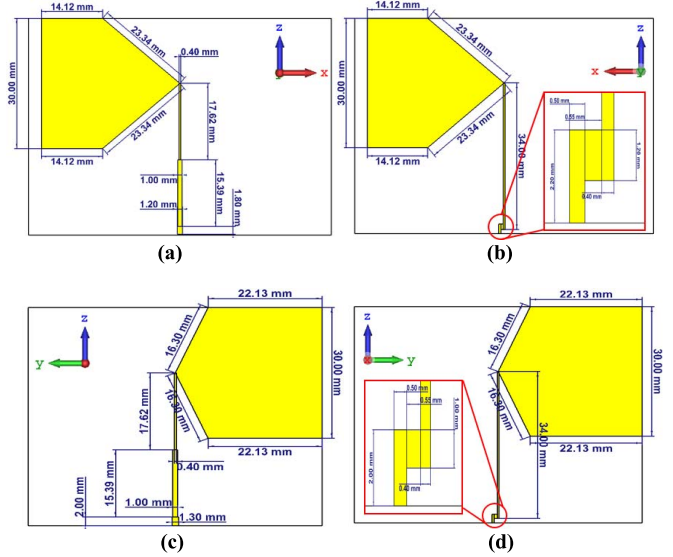


Fig. 3. Dimension of PCB. (a) Front side of HP. (b) Back side of HP. (c) Front side of VP. (d) Back side of VP.

and the ferrite sheet only satisfies the boundary condition of VP dipoles (y -direction polarized) as a PMC wall. Based on those conditions, the dimensions of a dual-polarized 1-D TCDA can be reduced.

III. DESIGN OF THE PROPOSED ARRAY ANTENNA

The configurations of the simulated unit cell antenna and the full array structure are shown in Fig. 2. The dimensions in Fig. 2(a) are as follows: $L = 60 \text{ mm}$, $W = 220 \text{ mm}$, $H = 50 \text{ mm}$, $W_f = 0.25 \text{ mm}$, $D = 15 \text{ mm}$, $U = 70 \text{ mm}$, $C_{vp} = 1.5 \text{ mm}$, $C_{hp} = 1.5 \text{ mm}$, $d = 1 \text{ mm}$, $g = 5 \text{ mm}$, and $g = 0.5 \text{ mm}$. The dimensions in Fig. 2(b) are as follows: $h_{sup1} = 19.08 \text{ mm}$, $h_{sup2} = 3.18 \text{ mm}$, and $h_0 = 27.74 \text{ mm}$. Fig. 2(c) shows the enlarged VMS structure. There are gaps in the VMSs. Without these gaps, the VMS acts as a monopole antenna with a resonance in the TCDA operation bandwidth, which makes the impedance matching poor. This unit cell antenna is simulated when it is infinitely periodic along the y axis. This antenna is also fed by a single-ended coaxial cable. To obtain the wideband characteristic, a superstrate with two layers was used. The superstrate (thickness = 22.26 mm) was stacked with Taconic TLY-5 ($\epsilon_r = 2.2$, $\tan \delta = 0.0009$, and thickness = h_{sup1}) and Taconic RF-35A ($\epsilon_r = 3.5$, $\tan \delta = 0.0016$, and thickness = h_{sup2}) dielectric material. The dimensions of the TLY-5 PCB for VP and HP dipoles are shown in Fig. 3. A bow-tie dipole antenna was used, and the feeding line comprised a stepped impedance line on the front side of the PCB.

A. Modification of the Side Walls

When designing the unit cell at a specific frequency, resonance can occur on the side walls when the length of a unit side wall is approximately one effective wavelength, i.e., 1.6 GHz in this case. This resonance degrades the radiation efficiency because strong magnetic losses occur on the ferrite sheets, especially for parts with high power losses, as shown

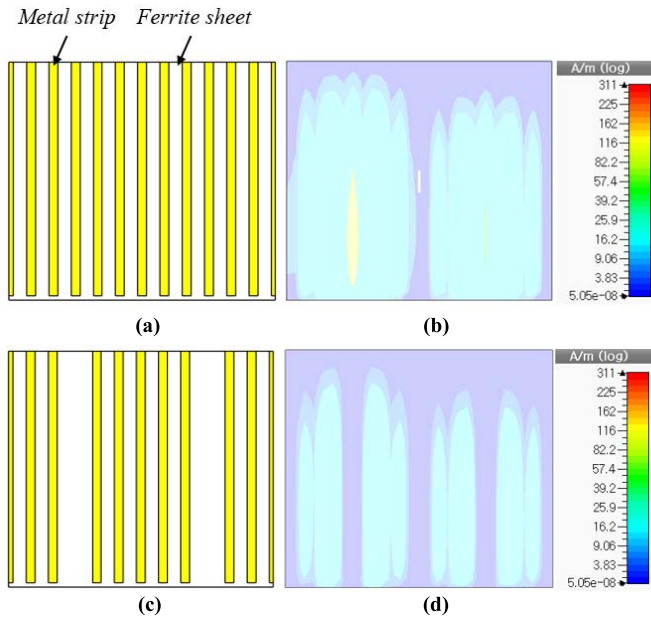


Fig. 4. (a) Configuration of the conventional side wall. (b) Power loss density on the ferrite sheet. (c) Configuration of the modified side wall. (d) Power loss density on the ferrite sheet.

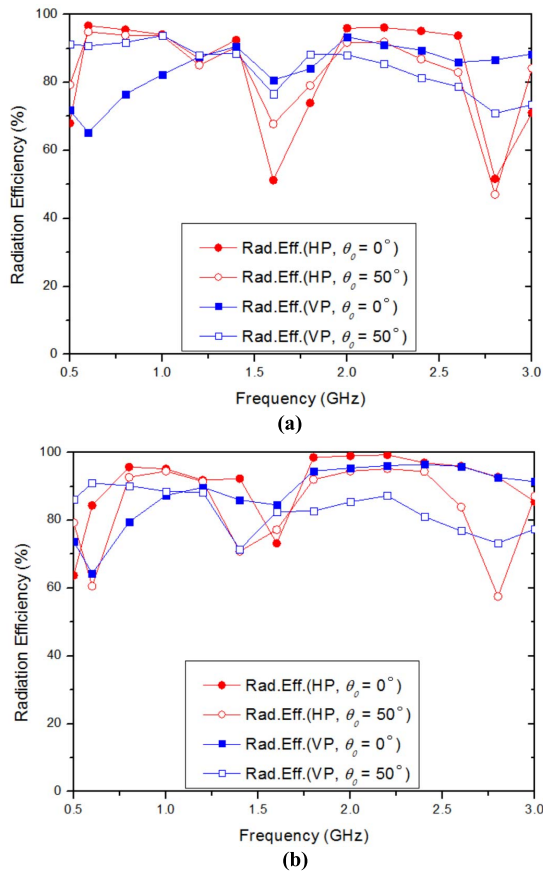


Fig. 5. Radiation efficiency of the (a) conventional and (b) proposed array antennas for both polarizations.

in Fig. 4(b). Therefore, the metal strips corresponding to the high power losses were removed, and the radiation efficiency improved from 51% to 73% at the resonance frequency,

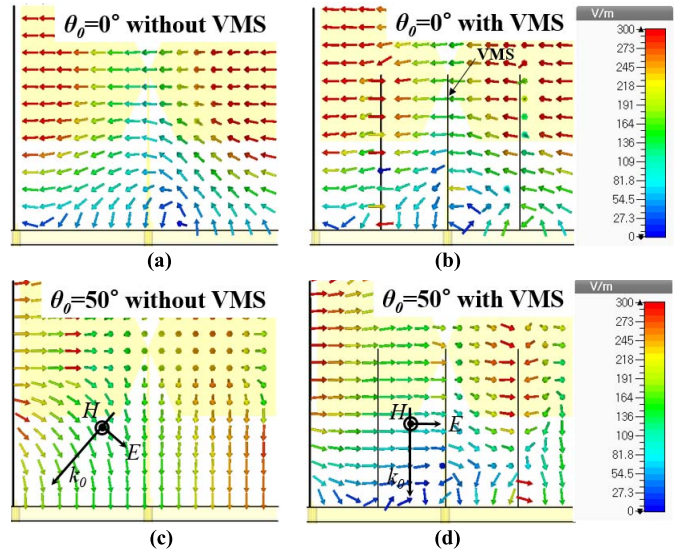


Fig. 6. yz plane from Fig. 2(b). Only VP dipoles are excited at 0.8 GHz and the TM mode is dominant. Electric field profile (a) without VMSs and (b) with VMSs, both when scanning the beam at $\theta_0 = 0^\circ$. Electric field profile (c) without VMSs and (d) with VMSs, both when scanning the beam at $\theta_0 = 50^\circ$.

as shown in Fig. 5. The radiation efficiency was over 70% within the operating IBW. The height of the side wall was chosen experimentally to be low for better impedance matching. Due to the fact that only two strips per sheet were removed, the impedance matching characteristic is slightly affected.

B. Implementation of a Low-Profile Array Antenna

As mentioned in Section II, when scanning the beam, the impedance matching was poor because the impedance is matched when scanning to the broadside, when the propagation mode was the TEM mode, which means that the electric and magnetic fields were perpendicular to the z -axis. As shown in Fig. 6(a) and (c), however, k_{z00}^- decreased when scanning to the other direction.

However, if the VMSs are established at proper positions, only the transverse electric and magnetic fields exist in the VMS region with $k_{z00}^- = k_0$, even when scanning the beam along the E-plane, as explained in [22]. It means that the TM mode (not TE mode) incident on the VMS region is converted into the special transmission-like mode, with $k_{z00}^- = k_0$ in VMS region as shown in Fig. 6(d) so that the electrical length between the dipole and the ground plane is not a function of the scanangle. Also, $Z^H(\theta_0)$ can be shown to be 377Ω with any scanangles. As a result, the array antenna with VMS can operate as a low-profile antenna since (8) is constant with scanangles.

In addition, 1-D TCDA was implemented using impedance surface walls made for both polarizations, where VP dipoles see only metal strips as PEC wall and HP dipoles see only ferrite sheets as PMC wall. However, when scanning the beam and steering the field profile, they are no longer the intended boundary surface walls and the impedance matching is poorer. However, by the proposed method, it can be improved.

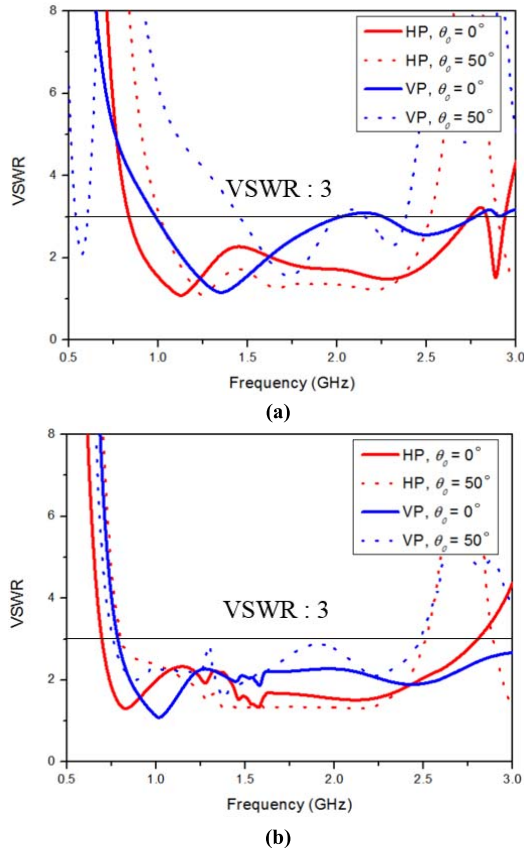


Fig. 7. Simulated VSWR of the antenna (a) without VMSs and (b) with VMSs.

Fig. 7 shows the simulated VSWR for both polarizations. At a low-frequency band, the impedance matching without VMSs was very poor, but the impedance matching with VMSs improved significantly, even at other frequencies. As a result, the height was reduced from $0.24\lambda_{\text{low}}$ to $0.13\lambda_{\text{low}}$ when scanning up to 50° at the lowest operating frequency for $\text{VSWR} < 3$ within the overlapped band. Furthermore, the operating IBW was 0.8–2.5 GHz (3.1:1).

IV. SIMULATED AND EXPERIMENTAL RESULTS FOR THE PROPOSED FULL ARRAY ANTENNA

The prototype of the full array antenna is shown in Fig. 8. The dimensions are $635 \times 220 \times 50 \text{ mm}^3$. There are 10 and 11 VP and HP dipoles, respectively, which are different for symmetric configuration. The superstrates are supported by Rohacell materials whose relative permittivity is nearly one.

The EM simulation of the proposed full array antenna was performed by the CST commercial EM tool. The radiation pattern of the array antenna was measured in an anechoic chamber.

The normalized gain pattern is shown in Fig. 9. On both the xz plane and the yz plane, the measurement results were in good agreement with the simulation results. In addition, the beamwidth was slightly wider when scanning the beam, and it became narrower as the frequency increased. Note that even though the VMSs were positioned between the dipoles, the radiation pattern was not odd. The measurement process

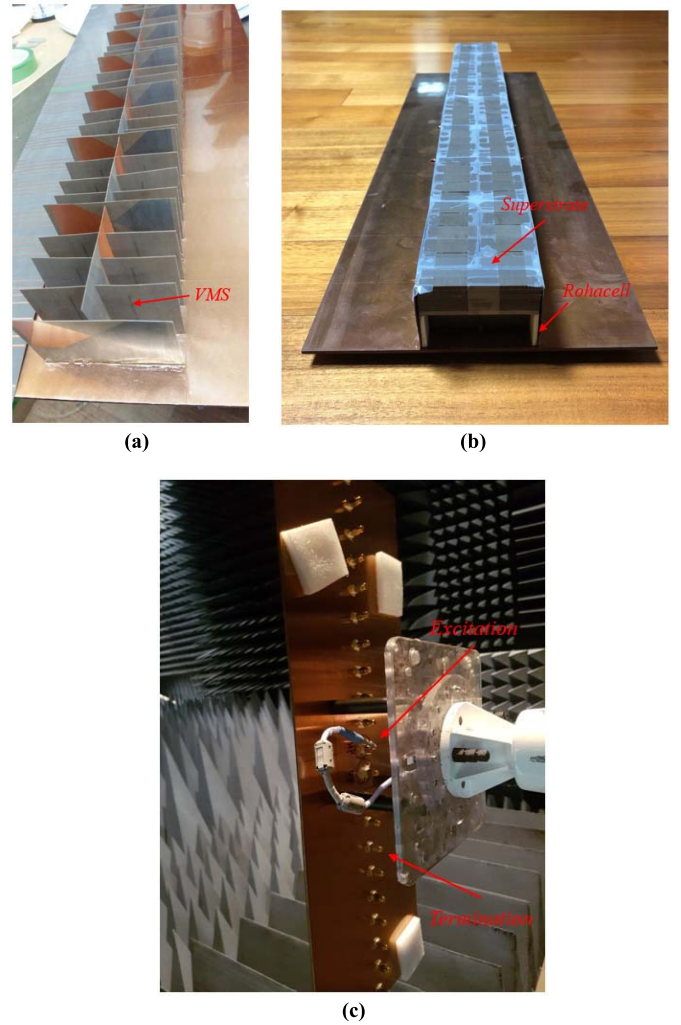


Fig. 8. Configuration of the proposed array antenna (a) without and (b) with superstrates. (c) Measurement setting, only one port is excited and others are 50Ω matched terminated.

was based on the superposition of the active element pattern [23]. In this method, one port is excited, and the others are matched terminated, as shown in Fig. 8(c). Then, the pattern is the active element pattern, which considers mutual coupling effects. In this way, all ports are performed individually. Finally, the superposition of each result was the total radiation pattern for both HPs and VPs. This procedure was performed using the following:

$$E(\theta, \phi) = \sum_{i=1}^N V_i g_i(\theta, \phi) \quad (9)$$

where V_i is the complex value of excitation, i is the number of ports, and $g_i(\theta, \phi)$ is the active element gain pattern of the i th element. The beam can be steered by inputting a phase to V_i .

The half power beam width (HPBW) for both polarizations is shown in Fig. 10. For VP, the HPBW was wider than 85° on the xz plane and narrower than 43° on the yz plane within the operating IBW. For HP, the HPBW was wider than 57° and narrower than 40° on the yz plane within the operating

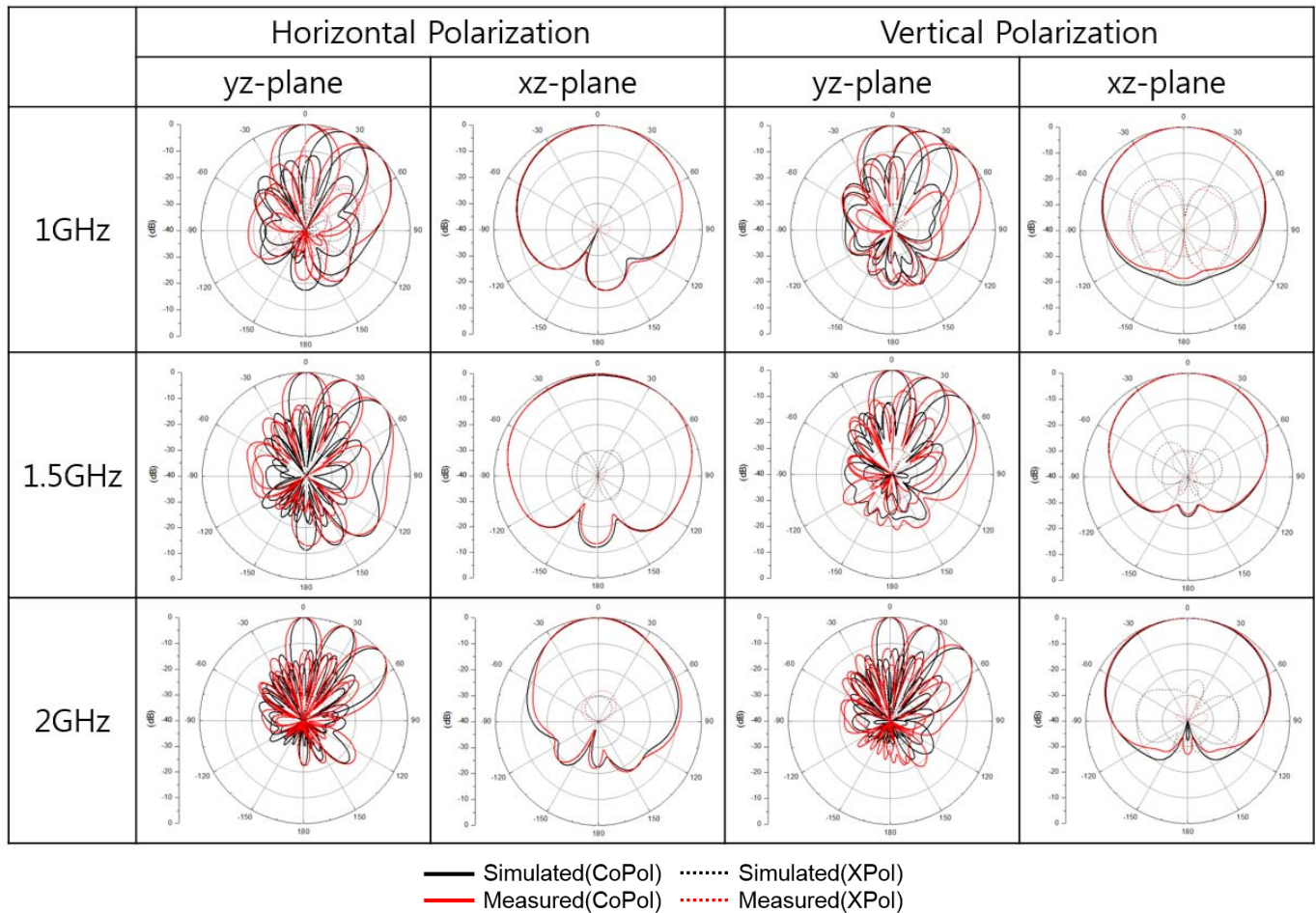


Fig. 9. Simulated and measured normalized gain patterns of the proposed array antenna for both polarizations on the xz plane and when scanning the beam to $\theta_0 = 0^\circ, 25^\circ,$ and 50° on the yz plane.

TABLE I
COMPARISON OF PERFORMANCES OF WIDEBAND, LOW-PROFILE, AND WIDE-SCANNING 1-D TCDA ANTENNAS

Ref.	Dimension (mm)	Height (λ_{low})	IBW (GHz, ratio, reference)	HPBW on xz plane ($^\circ$)	Polarization	Gain (dB)	Scan-angle ($^\circ$)
[12]	600×200	0.23	1.16–2.57, 2.2:1, VSWR < 2.3	> 61	Dual	> 8.6 8 VP elements 9 HP elements	< ± 30
[13]	1949×67	0.15 ¹⁾	0.45–2.05, 4.6:1 VSWR < 3	NG	Dual	> 11.7 (1, 2 GHz) 26 elements (VP/HP)	< ± 60
[14]	$140 \times \text{NG}$	0.21 ¹⁾	2.2–6, 2.7:1, VSWR < 2	NG	Single	> 6.7 8 VP elements	< ± 45
This Work	635×220	0.13	0.8–2.5, 3.1:1 VSWR < 3	> 57	Dual	> 7 10 VP elements 11 HP elements	< ± 50

*NG: Not Given

¹⁾ Calculated by excluding external power dividers or combiners

IBW. Because the number of VP dipoles was smaller than the number of HP dipoles, the HPBW of a HP was narrower than the HPBW of a VP, on average.

The peak gains are shown in Fig. 11. The measured gain was slightly smaller than the simulated results. However,

the total trend was very similar. In addition, it should be noted that the gain at 0.8 GHz was not low due to good impedance matching at the frequency. The measured gain was over 7 dB for VP and 7.3 dB for HP when scanning up to 50° . In addition, when scanning the beam, the gain was degraded

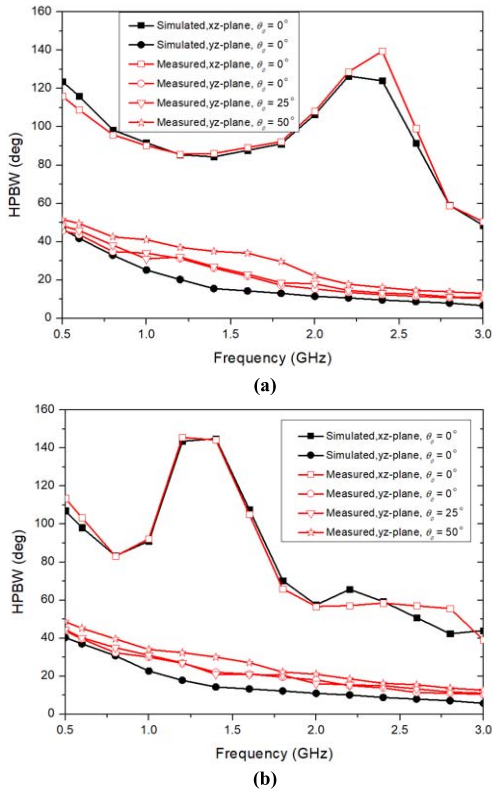


Fig. 10. Simulated and measured HPBW of the proposed array antenna for (a) VP and (b) HP.

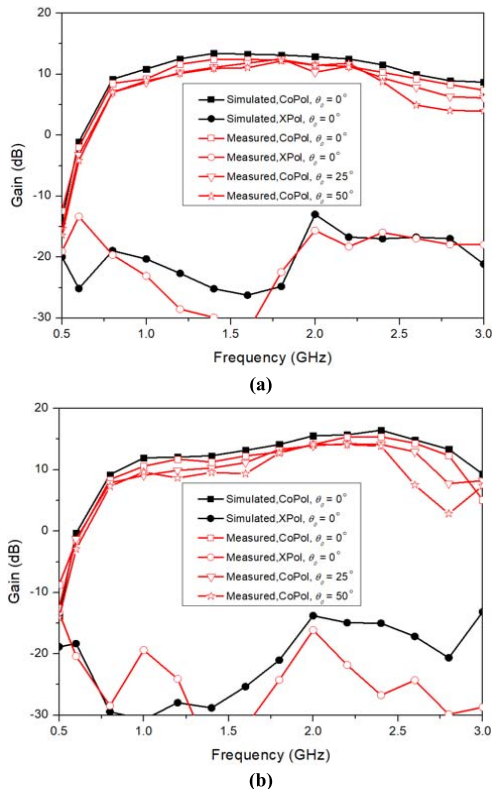


Fig. 11. Simulated and measured CoPol/XPoL gains of the proposed array antenna for (a) VP and (b) HP.

due to the scan loss. The measured cross-polarization level for VP was less than -15 dB and less than -16 dB for HP when scanning the broadside within the operating IBW.

Table I shows the comparison with wideband, low-profile, 1-D array antennas. The proposed array antenna is a dual-polarized, wideband, low-profile antenna without an integrated balun and a power divider or combiner [10]. Therefore, this method can be expected to be used for many applications.

V. CONCLUSION

In this paper, we proposed a wideband low-profile 1-D TCDA antenna using VMSs. We employed Floquet theory to describe the main reason for impedance mismatching when scanning the beam. This was confirmed by the field profile between the dipole and the ground plane, but the VMSs did not change the field profile. As a result, IBW for VSWR < 3 was 0.8–2.5 GHz (3.1:1), and the antenna's height was reduced from $0.24\lambda_{\text{low}}$ to $0.13\lambda_{\text{low}}$. The measurement results of the proposed array antenna were also in good agreement with the simulation results. This array antenna can be used in 1-D phased array antenna systems (e.g., base station array antennas or electronic warfare array antennas). This concept is expected to be used not only for array antennas but also for single vertical antennas with a ground plane, thus providing a low-profile characteristic.

REFERENCES

- [1] P. J. Gibson, "The Vivaldi aerial," in *Proc. 9th Eur. Microw. Conf.*, Sep. 1979, pp. 101–105.
- [2] H. Holter, T.-H. Chio, and D. H. Schaubert, "Experimental results of 144-element dual-polarized endfire tapered-slot phased arrays," *IEEE Trans. Antennas Propag.*, vol. 48, no. 11, pp. 1707–1718, Nov. 2000.
- [3] M. Kragalott, W. R. Pickles, and M. S. Kluskens, "Design of a 5:1 bandwidth stripline notch array from FDTD analysis," *IEEE Trans. Antennas Propag.*, vol. 48, no. 11, pp. 1733–1741, Nov. 2000.
- [4] R. W. Kindt and W. R. Pickles, "Ultrawideband all-metal flared-notch array radiator," *IEEE Trans. Antennas Propag.*, vol. 58, no. 11, pp. 3568–3575, Nov. 2010.
- [5] J. Bang, J. Lee, and J. Choi, "Design of a wideband antipodal Vivaldi antenna with an asymmetric parasitic patch," *J. Electromagn. Eng. Sci.*, vol. 18, no. 1, pp. 29–34, Jan. 2018.
- [6] S. J. Yoon and J. Choi, "A low-profile broadband array antenna for home repeater applications," *J. Electromagn. Eng. Sci.*, vol. 18, no. 4, pp. 261–266, Oct. 2018.
- [7] J. L. Volakis and K. Sertel, "Narrowband and wideband metamaterial antennas based on degenerate band edge and magnetic photonic crystals," *Proc. IEEE*, vol. 99, no. 10, pp. 1732–1745, Oct. 2011.
- [8] B. Munk, *Finite Antenna Arrays and FSS*. Hoboken, NJ, USA: Wiley, 2003.
- [9] S. S. Holland and M. N. Vouvakis, "The planar ultrawideband modular antenna (PUMA) array," *IEEE Trans. Antennas Propag.*, vol. 60, no. 1, pp. 130–140, Jan. 2012.
- [10] J. P. Doane, K. Sertel, and J. L. Volakis, "A wideband, wide scanning tightly coupled dipole array with integrated balun (TCDA-IB)," *IEEE Trans. Antennas Propag.*, vol. 61, no. 9, pp. 4538–4548, Sep. 2013.
- [11] D. K. Papantoni and J. L. Volakis, "Dual-polarized tightly coupled array with substrate loading," *IEEE Antennas Wireless Propag. Lett.*, vol. 15, pp. 325–328, 2015.
- [12] H. Lee and S. Nam, "A dual-polarized 1-D tightly coupled dipole array antenna," *IEEE Trans. Antennas Propag.*, vol. 65, no. 9, pp. 4511–4518, Sep. 2017.
- [13] H. Zhang, S. Yang, Y. Chen, J. Guo, and Z. Nie, "Wideband dual-polarized linear array of tightly coupled elements," *IEEE Trans. Antennas Propag.*, vol. 66, no. 1, pp. 476–480, Jan. 2018.
- [14] Y. Wang, L. Zhu, H. Wang, Y. Luo, and G. Yang, "A compact, scanning tightly coupled dipole array with parasitic strips for next-generation wireless applications," *IEEE Antennas Wireless Propag. Lett.*, vol. 17, no. 4, pp. 534–537, Apr. 2018.

- [15] J. Zhong, C. W. Lee, D. Papantoni, A. Kiourti, and J. L. Volakis, "Body-worn 30:1 bandwidth tightly coupled dipole array on conductive textiles," *IEEE Antennas Wireless Propag. Lett.*, vol. 17, no. 5, pp. 723–726, May 2018.
- [16] E. Magill and H. Wheeler, "Wide-angle impedance matching of a planar array antenna by a dielectric sheet," *IEEE Trans. Antennas Propag.*, vol. AP-14, no. 1, pp. 49–53, Jan. 1966.
- [17] T. R. Cameron and G. V. Eleftheriades, "Analysis and characterization of a wide-angle impedance matching metasurface for dipole phased arrays," *IEEE Trans. Antennas Propag.*, vol. 63, no. 9, pp. 3928–3938, Sep. 2015.
- [18] E. Yetisir, N. Ghalichechian, and J. L. Volakis, "Ultrawideband array with 70° scanning using FSS superstrate," *IEEE Trans. Antennas Propag.*, vol. 64, no. 10, pp. 4256–4265, Oct. 2016.
- [19] H. Wheeler, "Simple relations derived from a phased-array antenna made of an infinite current sheet," *IEEE Trans. Antennas Propag.*, vol. AP-13, no. 4, pp. 506–514, Jul. 1965.
- [20] A. K. Bhattacharyya, *Phased Array Antennas: Floquet Analysis, Synthesis, BFNs and Active Array Systems*, vol. 179. Hoboken, NJ, USA: Wiley, 2006.
- [21] H. A. Wheeler, "The radiation resistance of an antenna in an infinite array or waveguide," *Proc. IRE*, vol. 36, no. 4, pp. 478–487, Apr. 1948.
- [22] P. A. Belov *et al.*, "Strong spatial dispersion in wire media in the very large wavelength limit," *Phys. Rev. B, Condens. Matter*, vol. 67, no. 11, Mar. 2003, Art. no. 113103.
- [23] D. F. Kelley and W. L. Stutzman, "Array antenna pattern modeling methods that include mutual coupling effects," *IEEE Trans. Antennas Propag.*, vol. 41, no. 12, pp. 1625–1632, Dec. 1993.



Seongjung Kim received the B.S. degree in electronic and electrical engineering from Hongik University, Seoul, South Korea, in 2017. He is currently pursuing the integrated master's and Ph.D. degree with the Department of Electrical Engineering and Computer Science, Seoul National University, Seoul.

His current research interests include metamaterial-based antennas and phased array antennas.



Sangwook Nam (S'87–M'88–SM'11) received the B.S. degree in electrical engineering from Seoul National University, Seoul, South Korea, in 1981, the M.S. degree in electrical engineering from the Korea Advanced Institute of Science and Technology (KAIST), Seoul, in 1983, and the Ph.D. degree in electrical engineering from the University of Texas at Austin, Austin, TX, USA, in 1989.

From 1983 to 1986, he was a Researcher with the Gold Star Central Research Laboratory, Seoul. Since 1990, he has been a Professor with the School

of Electrical Engineering and Computer Science, Seoul National University. His current research interests include the analysis/design of electromagnetic structures, antennas, and microwave active/passive circuits.